Chemically Selective Imaging of Subcellular Structure in Human Hepatocytes with Coherent Anti-Stokes Raman Scattering (CARS) Near-Field Scanning Optical Microscopy (NSOM)

Richard D. Schaller,[†] Joseph Ziegelbauer,[‡] Lynn F. Lee,[†] Louis H. Haber,[†] and Richard J. Saykally*,[†]

Department of Chemistry, University of California, Berkeley, California 94720-1460 and Department of Molecular and Cellular Biology, University of California, Berkeley, California 94720-3204

Received: April 1, 2002; In Final Form: May 24, 2002

We demonstrate the combination of coherent anti-Stoke Raman scattering (CARS) with near-field scanning optical microscopy (NSOM) for chemically selective imaging via intrinsic vibrational resonances with spatial resolution below the diffraction limit. Femtosecond, near-IR pulses are used to produce CARS signals from human hepatocytes, and by tuning the CARS signal to be resonant with C−H stretching frequencies, image contrast is observed with an optical spatial resolution of ∼128 nm.

The development of chemically selective imaging techniques is attracting much attention due to the many possible applications in biology and nanoscience. Raman[1−5] and infrared microscopies[1,6−10] are both of interest because they can exploit intrinsic vibrational chromophores, thus potentially obviating the need for staining and incorporation of fluorescent probes. However, the former is relatively insensitive and requires high laser powers while the latter engenders relatively high background and low optical contrast. Advances in employing coherent anti-Stokes Raman scattering (CARS) for high spatial resolution far-field microscopy has attracted much recent interest.[11−20] CARS imaging can probe a sample with higher sensitivity than spontaneous Raman and IR methods, as it is a coherent process (the signal is proportional to the square of the number of chromophores). Moreover, the optical contrast can also be higher since resonant enhancement of this third-order process can be as large as 10^4 to 10^6.[21]

CARS results from mixing incident pump (ω_P) and Stokes (ω_S) frequencies to produce a third-order induced polarization ($P^{(3)}$) within a sample at an anti-Stokes frequency (ω_{AS}) as described by

$$P_i^{(3)}(\omega_{AS}) = \chi_{ijkl}^{(3)}(\omega_{AS} = \omega_P - \omega_S + \omega_P)E_j(\omega_P)\, E_k(\omega_P)\, E_l(\omega_S) \quad (1)$$

Here, $\chi^{(3)}$ is the third-order susceptibility of a sample that couples the electric fields of the input pulses. As with other nonlinear processes, the total third-order susceptibility associated with a CARS process consists of both resonant and nonresonant components,

$$\chi_{total}^{(3)} = \chi_R^{(3)} + \chi_{NR}^{(3)} \quad (2)$$

The resonant component can be described, within the context of vibrationally resonant CARS, as[16,21]

$$\chi_R^{(3)} = \frac{a}{(\omega_P - \omega_S) - \omega_v + i\Gamma_v} \quad (3)$$

where a is a constant containing Raman cross-section values and mode densities, and 2Γ is the line width associated with the resonant vibrational frequency ω_v. The resonant component of the total $\chi^{(3)}$ response can become very large when the difference in energy between the pump and Stokes pulses becomes equal to a Raman active vibrational frequency within a sample,[21] yielding a 10^4 to 10^6 increase in efficiency. This large resonance enhancement can thus provide high optical contrast in imaging.

A significant impediment to CARS measurements, however, is the presence of background at the same frequency as the CARS signal. This background is thought to be due to the CARS process accessing electronic resonances or preresonances produced by an initial summation of two pump pulses, which may be resonant with electronic excited states in a sample, followed by a difference frequency generation process with the Stokes pulse.[13] Such electronic resonances can occur in addition to vibrational resonances, thus obscuring the desired vibrational information. The completely nonresonant portion of the total $\chi^{(3)}$ can also be a nonnegligible component of the total CARS signal.[21]

Extensive efforts to reduce these undesirable, vibrationally nonresonant contributions to the total CARS signals have been made. The most important of these involves the use of red or near-IR incident laser pulses to reduce the effect of electronically resonant CARS processes. Xie et al. have shown that epi-detection of CARS signals in far-field microscopy can reduce the contribution of signal levels from solvent molecules[16,17] and polarization control of the input frequencies combined with polarization analysis of CARS signals further suppresses background.[18,21] These efforts have resulted in an improved ratio of resonant to background CARS signal contributions in far-field microscopy.

The spatial resolution of far-field CARS microscopy, however, is intrinsically limited by diffraction of the pump pulse to $\sim\lambda_{PUMP}/2$. In this study, we explore the combination of CARS with near-field scanning optical microscopy (NSOM) as a means to transcend this intrinsic limit on spatial resolution. NSOM

* To whom correspondence should be addressed. E-mail: saykally@cchem.berkeley.edu.
[†] Department of Chemistry.
[‡] Department of Molecular and Cellular Biology.

10.1021/jp020855t CCC: $22.00
Published on Web 07/25/2002

provides spatial resolution that is predominantly determined by the diameter of a nanoscopic fiber probe tip.[22−24] The maintenance of near-field feedback can also be used to simultaneously generate a topographical image of the sample that can be compared with the optical signals. The probe collects optical signals produced by a sample in the electromagnetic near-zone before high spatial frequency information contained in signal evanescent waves is lost via far-field diffraction. Furthermore, phase-matching is relaxed in near-field detection of coherent nonlinear optical signals, as the fields are collected before propagation results in destructive interference and cancellation of signals in non-phase-matched directions.[25,26]

Due to phase-matching relaxation, CARS NSOM techniques cannot exploit some of the methods used to reduce background CARS signals. In particular, the epi-detection scheme, which has been shown to reduce background signal levels from solvent molecules in far-field microscopy studies,[16,17] is not applicable to CARS NSOM, as interference, which is the basis of the epi-detection scheme, does not occur over the short distances of the nonlinear source field to the near-field detector.

The near-field detected CARS signal intensity (I_{CARS}), which is proportional to the square of the generated third-order induced polarization, for an oblique collection mode NSOM experimental geometry can be expressed as the far-field signal intensity[21] attenuated by near-field microscopy terms.[27]

$$I_{CARS} \propto |\vec{\chi}^{(3)}|^2 I_P^2 I_S \left(\frac{r}{\lambda}\right)^6 [\int_0^l e^{-(T+S)/k\lambda}\, dS]^2 \qquad (4)$$

where I_i (i = P and S) is the intensity of the pump and Stokes laser pulses, r is the radius of the probe tip, λ is the wavelength of the detected photons, k is a material-specific barrier to tunneling, l is the NSOM depth of field, T is the length of the taper region from the probe tip to wavelength dimensions in the fiber optic, and S is the distance of nonlinear sources to the probe tip. The $(r/\lambda)^6$ term describes the optical transmission efficiency of a subwavelength aperture and signifies a sacrifice of optical signal for increased spatial resolution, while the exponential term models the photon transmission through the subwavelength probe as a tunneling event that results in a shallow depth of field.[22−24] These combined near-field effects typically attenuate far-field signal levels by $\sim 10^4$ when chemically etched NSOM probes are utilized as in this work.

We have previously utilized third harmonic generation (THG), a third-order process in which three degenerate photons are combined in a sample to produce one photon of 3 times higher energy, combined with NSOM and the tunability of a titanium: sapphire laser source to demonstrate that chemical image contrast can be generated in NSOM imaging by tuning the laser onto 3ω resonances of chromophores within the sample.[28] We have also used this nonlinear chemical imaging method to study ground-state interchain nanodomains contained within films of conjugated polymers.[29]

In the following study, we demonstrate CARS NSOM and show that resonantly enhanced near-field CARS signals are observable and can provide a useful chemical contrast mechanism for subdiffraction spatial resolution imaging. Background signals are indeed present in our measurements; however, we observe stronger CARS signals from vibrationally resonant processes. We demonstrate this technique on human hepatocytes with resonantly enhanced vibrational contrast generated by C−H-containing moieties thought to be concentrated in the mitochondrial reticulum.

The experimental design of the CARS NSOM experiment is shown in Figure 1.

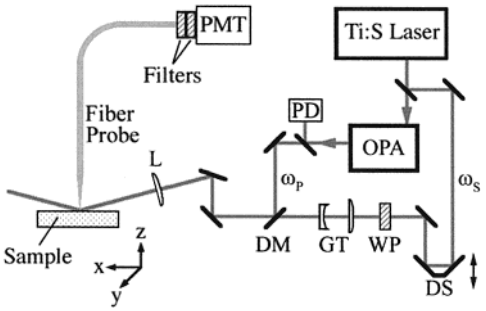

Figure 1. Experimental setup: silicon photodiode (PD), dichroic mirror (DM), delay stage (DS), zero-order half-waveplate (WP), Galilean telescope (GT), 10 cm focal length singlet lens (L). Stokes pulses (ω_S, fixed at 805 nm) and tunable pump pulses (ω_P, tunable between 600 and 805 nm) generated via an optical parametric amplifier (OPA) were used to produce CARS signals. Photons collected by a chemically etched, uncoated NSOM fiber probe were directed to broad band-pass filters and detected with a Hamamatsu 3896 photomultiplier tube (PMT) biased at −1100 V and fast gated electronics. Sample stage piezos perform the *x*, *y*, and *z* directions of motion for both scanning and near-field feedback so that the NSOM probe experiences an invariant tip/field geometry. The tip to sample distance was maintained at ∼5 nm with shear-force feedback. All images are 200 × 200 pixel *x*, *y* arrays, *z* pixel values represent the average of 45 laser shots, and images have not been processed.

A commercial NSOM (TMmicroscopes, Lumina) equipped with a shear-force feedback mechanism was employed for near-field measurements of CARS signals. Fiber optic probes were chemically etched to a ∼50 nm diameter tip and were not metal coated. Topographical and optical signals were obtained simultaneously for comparison. The forward and reverse scanning motions of the sample (the tip remains static in the laboratory frame) were collected to produce separate images as a check of reproducibility. Repeatable optical images were then added together to reduce random noise.

The light source for the experiments consisted of a home-built titanium:sapphire oscillator (800 nm, 480 mW, 30 fs, 88 MHz) which was used to seed a commercial (Spectra-Physics) chirped pulse amplifier (805 nm, 2.25 W, 100 fs, 1 kHz). This output was beamsplit 90:10, using 90% to pump a commercial (Quantronix, Topaz) superfluorescence optical parametric amplifier (OPA) (1.16−2.7 μm, 300 μJ at 1350 nm, 100 fs). Tunable visible/near-IR wavelengths (ω_P) were produced via second harmonic generation of the OPA signal output in a BBO crystal (600−800 nm, 70 μJ, 100 fs) and were further attenuated to 0.7 μJ using a variable neutral density filter. The residual 10% of the amplifier output, utilized as the Stokes pulse (ω_S) for these measurements, was attenuated to 1 μJ, controlled for polarization with a zero-order half-waveplate, directed through a Galilean telescope, and made to propagate collinearly with the tunable pump pulse train via a dichroic mirror. The *p*-polarized pump and Stokes pulses were focused to a ∼100 μm diameter spot centered at the position where the fiber probe investigated the sample with a 10 cm focal length plano-convex singlet lens and were overlapped in time by adjusting the Stokes pulse timing with a manual delay line. Signals collected by the near-field probe were directed to broad band-pass filters and detected with a photomultiplier tube (PMT) and boxcar integrator. Typically 0−4 CARS photons were detected per laser shot[30] and complete images required ∼30 min to collect. Normalization of shot-to-shot instabilities in CARS signals was performed by mathematically squaring the output of a silicon photodiode that was used to monitor the doubled output of the OPA.

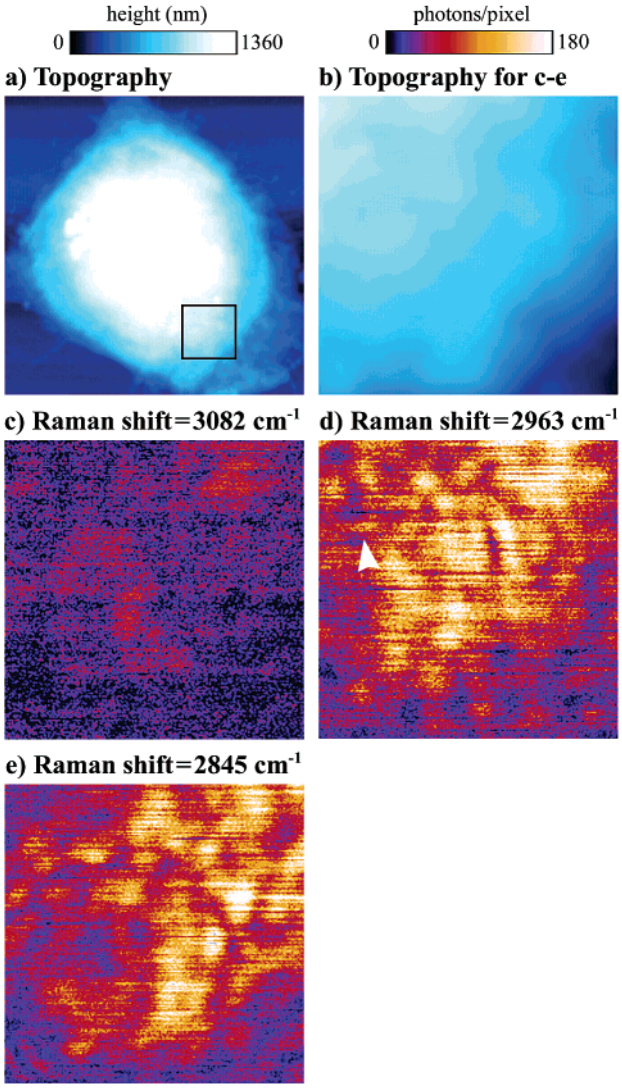

Figure 2. CARS NSOM images of human hepatocytes. (c−e) CARS NSOM images of an (4.3 μm)^2 area of a human hepatocyte produced at Stokes-shifted energies of 3082, 2963, and 2845 cm^{-1}, respectively, for the same topographical area shown in (b). Stronger signal levels and optical contrast are observed in (d) and (e), in which the Stokes shift is resonant with vibrational C−H transition frequencies within the sample that are associated with the mitchondrial reticulum.

Human hepatocyte (HepG2) samples were incubated in wells over poly-L-lysine-treated, sterile, sapphire substrates for 30 min at room temperature, rinsed with phosphate saline buffer (PBS), and then fixed with paraformaldehyde. Sapphire, rather than SiO_2, substrates were utilized, as the former produced lower background signal levels.

Shown in Figure 2c−e, are reproducible CARS NSOM images of a human hepatocyte produced using pump wavelengths of 645, 650, and 655 nm, respectively, and a fixed Stokes wavelength of 805 nm for the same (4.3 μm)^2 region is shown topographically in (b) (shown on a larger scale in (a)). It can be seen that very little optical contrast is observed in (c) when the resulting Stokes shift[31] is centered at ∼3082 cm^{-1}. Contrast, as well as nearly 3 times stronger CARS signals, are observed in (d) and (e), wherein the Stokes shifts are centered at ∼2963 and 2845 cm^{-1}, respectively.

We interpret the CARS NSOM image contrast shown in Figure 2d,e to result from intracellular structures exhibiting C−H vibrational resonances within the sample, as these typically occur in the experimental energy range of ∼3000−2800 cm^{-1}.[32] In

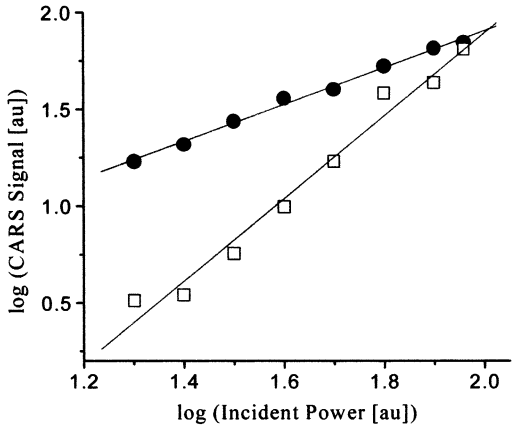

Figure 3. Signal power dependences. Power dependences of the near-field detected signals were determined with a stepped neutral density filter for a pump wavelength of 650 nm. Each data point represents the average of 21 000 laser shots. Linear fits to the data points in the log−log plots exhibit a slope equal to 1 (fit = 0.98 ± 0.05) for the Stokes pulses (circles) and a slope equal to 2 (fit = 2.08 ± 0.13) for the pump pulses (squares), as is expected for CARS.

particular, frequencies near 2930 cm^{-1} are associated with methyl stretches (−CH_3) while those near 2850 cm^{-1} are associated with methylene (−CH_2−) stretches. The CARS NSOM images reveal high density, reticulated features that appear on the submicron scale, as has recently been observed for mitochondria imaged with fluorescence labeling methods.[33,34] Far-field CARS images of human epithelial cells produced in the same Stokes shifted range by Zumbusch et al. have also been interpreted to result from mitochondrial organelle structures that contain high C−H bond concentrations.[13] Mitochondria occupy ∼20% of the cell volume in mammalian hepatocytes[35] and ∼75% of the lipids constituting their membranes are composed of phosphatidylcholine and phospatidylethanolamine, making these molecules the likely sources of the resonant enhancement.

The CARS NSOM image series in Figure 2 shows that while background CARS signals are present in near-field detected CARS, these do not overwhelm signal generated from the desired resonant processes. The bluest pump frequency used (645 nm for Figure 2c), would be more likely to excite electronic resonances than would the redder pump pulse, and yet the CARS signal levels are lower than those in (d) and (e) that used redder pump wavelengths. Background signals resulting from the nonresonant component of $\chi^{(3)}$ should not vary significantly over this small spectral range. Moreover, signal levels in (c) may not result entirely from electronic resonance. Vibrational O−H resonances from water in the cytosol are very broad and may also be a source of vibrationally resonant CARS photons (especially in (c)) but do not result in optical contrast for this sample.

To demonstrate that the signals observed in Figure 2 actually result from the CARS process, power dependences of signals were measured.[13] Figure 3 shows near-field detected power dependences of the optical signals for both the pump and Stokes pulses, produced using a stepped neutral density filter. As expected for the CARS process, a linear signal dependence is observed for the Stokes pulse that only involves one photon in the CARS process while the pump pulse shows a second-order dependence as two photons of this wavelength are involved. For this reason, we can confirm that we are indeed observing CARS mixing in the hepatocytes. The coherent nonlinear signals are detectable in a non-phase-matched direction because, as in our previous nonlinear NSOM studies,[27,28,36−38] they are col-

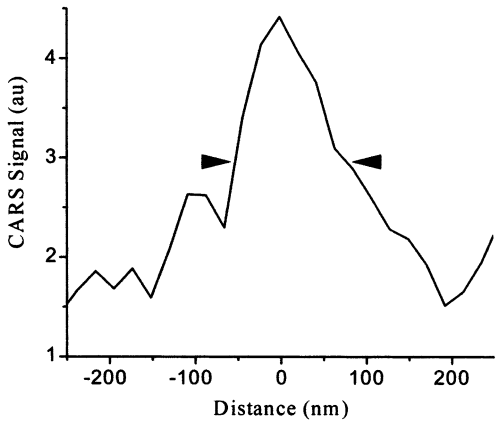

Figure 4. CARS NSOM spatial resolution. A line trace through the region denoted by an arrow in Figure 2d shows a fwhm of ~128 nm. This is similar to the spatial resolution that we have observed in other nonlinear NSOM experiments employing uncoated NSOM tips.[27,38]

lected in the near-field for which phase-matching conditions are relaxed.[25,26]

A line trace through the CARS NSOM image shown in Figure 2d is shown in Figure 4. The fwhm of this feature is ~128 nm, similar to what we have observed in previous studies that combine nonlinear optical signal generation with NSOM detection in this geometry.[27,38]

We have also performed CARS NSOM using a noncollinear pulse geometry identical to that described in our recent SFG NSOM study.[37] Both experimental designs resulted in comparable CARS NSOM signal levels; however, the complexity of alignment is significantly reduced using the collinear approach, given the similar wavelength range of the pulses.

Clearly, higher spectral resolution will be required to image samples with higher chemical specificity, especially as we begin to probe lower energy Stokes shifts, wherein vibrational bands become more closely spaced. Cheng et al. have calculated that pulses with less than ~10 cm^{-1} of bandwidth should maximize the ratio of resonant to nonresonant CARS signals for the specific case of a resonant absorber with $2\Gamma = 9.2$ cm^{-1}.[16] In the spectral region probed in the present study, however, which was also explored by Zumbusch,[13] the vibrational features that are exploited have a broadband structure and therefore may not exhibit the saturation effects that narrower vibrational resonances experience. Incorporation of multiplex methods that mix a picosecond, spectrally narrow laser pulse with a spectrally broad, femtosecond pulse can provide increased spectral resolution and high spectral coverage, as recently demonstrated in far-field[39−43] and near-field[27] sum frequency generation studies as well as recently in an elegant far-field CARS study by Muller et al.[19]

In summary, we have demonstrated the first CARS NSOM experiments and used the method to image a human hepatocyte using the intrinsic vibrational resonances of C−H-containing molecules found in subcellular structures. CARS signals were observed with <2 mW of total average laser power, which should be tolerable by most potential samples. We have achieved spatial resolution that is well below the diffraction limit with this method as well. This technique appears to hold promise as a general tool for microscopy and should find useful applications in biology and nanoscience.

Acknowledgment. This work was supported by the Experimental Physical Chemistry Division of the National Science Foundation, the National Institutes of Health (grant CA25417), and the Howard Hughes Medical Institute.

References and Notes

(1) Kalasinsky, V. F. *Appl. Spectrosc. Rev.* **1996**, *31*, 193−249.
(2) Deckert, V.; Zeisel, D.; Zenobi, R.; VoDinh, T. *Anal. Chem.* **1998**, *70*, 2646−2650.
(3) Jahncke, C. L.; Paesler, M. A.; Hallen, H. D. *Appl. Phys. Lett.* **1995**, *67*, 2483−2485.
(4) Labarthet, F. L.; Bruneel, J. L.; Buffeteau, T.; Sourisseau, C.; Huber, M. R.; Zilker, S. J.; Bieringer, T. *Phys. Chem. Chem. Phys.* **2000**, *2*, 5154−5167.
(5) Narita, Y.; Tadokoro, T.; Ikeda, T.; Saiki, T.; Mononobe, S.; Ohtsu, M. *Appl. Spectrosc.* **1998**, *52*, 1141−1144.
(6) Wetzel, D. L.; LeVine, S. M. *Science* **1999**, *285*, 1224−1225.
(7) Piednoir, A.; Licoppe, C.; Creuzet, F. *Opt. Commun.* **1996**, *129*, 414−422.
(8) Knoll, B.; Keilmann, F. *Nature* **1999**, *399*, 134−137.
(9) Dragnea, B.; Preusser, J.; Szarko, J. M.; McDonough, L. A.; Leone, S. R.; Hinsberg, W. D. *Appl. Surf. Sci.* **2001**, *175*, 783−789.
(10) Michaels, C. A.; Stranick, S. J.; Richter, L. J.; Cavanagh, R. R. *J. Appl. Phys.* **2000**, *88*, 4832−4839.
(11) Duncan, M. D.; Reintjes, J.; Manuccia, T. J. *Opt. Lett.* **1982**, *7*, 350−2.
(12) Duncan, M. D. *Opt. Commun.* **1984**, *50*, 307−12.
(13) Zumbusch, A.; Holtom, G. R.; Xie, X. S. *Phys. Rev. Lett.* **1999**, *82*, 4142−4145.
(14) Muller, M.; Squier, J.; De Lange, C. A.; Brakenhoff, G. J. *J. Microsc.* **2000**, *197*, 150−8.
(15) Hashimoto, M.; Araki, T. *Opt. Lett.* **2000**, *25*, 1768−1770.
(16) Cheng, J. X.; Volkmer, A.; Book, L. D.; Xie, X. S. *J. Phys. Chem. B* **2001**, *105*, 1277−1280.
(17) Volkmer, A.; Cheng, J. X.; Xie, X. S. *Phys. Rev. Lett.* **2001**, *8702*, 3901-U47.
(18) Cheng, J. X.; Book, L. D.; Xie, X. S. *Opt. Lett.* **2001**, *26*, 1341−1343.
(19) Muller, M.; Schins, J. M. *J. Phys. Chem. B* **2002**, *106*, 3715−3726.
(20) Labarthet, F. L.; Shen, Y. R. Nonlinear optical microscopy. In *Advanced methods in contemporary optical systems and microscopy*; Kao, F. J., Torok, P., Eds.; Springer-Verlag: Berlin, Germany, in press.
(21) Shen, Y. R. *The Principles of Nonlinear Optics*; J. Wiley: New York, 1984.
(22) Dunn, R. C. *Chem. Rev.* **1999**, *99*, 2891−927.
(23) Betzig, E.; Trautman, J. K. *Science* **1992**, *257*, 189−95.
(24) Paesler, M. A.; Moyer, P. J. *Near-field Optics: Theory, Instrumentation, and Applications*; Wiley: New York, 1996.
(25) Vigoureux, J. M.; Girard, C.; Depasse, F. *J. Mod. Opt.* **1994**, *41*, 49−58.
(26) Xiaolin, Z.; Kopelman, R. *Ultramicroscopy* **1995**, *61*, 69−80.
(27) Schaller, R. D.; Johnson, J. C.; Wilson, K. R.; Lee, L. F.; Haber, L. H.; Saykally, R. J. *J. Phys. Chem. B* **2002**, *106*, 5143−54.
(28) Schaller, R. D.; Johnson, J. C.; Saykally, R. J. *Anal. Chem.* **2000**, *72*, 5361−5364.
(29) Schaller, R. D.; Snee, P. T.; Johnson, J. C.; Lee, L. F.; Wilson, K. R.; Haber, L. H.; Saykally, R. J.; Nguyen, T.-Q.; Schwartz, B. J. *J. Chem. Phys.*, in press.
(30) Observed signal levels were consistent with calculation using eq 4 with an effective $\chi^{(3)}$ of order 10^{-14} esu and a photon tunneling attenuation of 10^{-4}.
(31) Center positions of the Raman shifts are reported, though we point out that the femtosecond pulses have ~150 cm^{-1} of bandwidth.
(32) Gremlich, H.-U.; Yan, B. *Infrared and Raman spectroscopy of biological materials*; Marcel Dekker: New York, 2001.
(33) Rizzuto, R.; Pinton, P.; Carrington, W.; Fay, F. S.; Fogarty, K. E.; Lifshitz, L. M.; Tuft, R. A.; Pozzan, T. *Science* **1998**, *280*, 1763−1766.
(34) Margineantu, D.; Capaldi, R. A.; Marcus, A. H. *Biophys. J.* **2000**, *79*, 1833−49.
(35) Alberts, B. *Molecular Biology of the Cell*, 3rd ed.; Garland Publishers: New York, 1994.
(36) Schaller, R. D.; Roth, C.; Raulet, D. H.; Saykally, R. J. *J. Phys. Chem. B* **2000**, *104*, 5217−5220.
(37) Schaller, R. D.; Saykally, R. J. *Langmuir* **2001**, *17*, 2055−2058.
(38) Johnson, J. C.; Yan, H.; Schaller, R. D.; Petersen, P. B.; Yang, P.; Saykally, R. J. *Nano Lett.* **2002**, *2*, 279−83.
(39) Richter, L. J.; Petralli-Mallow, T. P.; Stephenson, J. C. *Opt. Lett.* **1998**, *23*, 1594−6.
(40) McGuire, J. A.; Beck, W.; Wei, X.; Shen, Y. R. *Opt. Lett.* **1999**, *24*, 1877−9.
(41) Bonn, M.; Hess, C.; Funk, S.; Miners, J. H.; Persson, B. N. J.; Wolf, M.; Ert, G. *Phys. Rev. Lett.* **2000**, *84*, 4653−6.
(42) Hess, C.; Funk, S.; Bonn, M.; Denzler, D. N.; Wolf, M.; Ertl, G. *Appl. Phys. A* **2000**, *A71*, 477−83.
(43) Briggman, K. A.; Stephenson, J. C.; Wallace, W. E.; Richter, L. J. *J. Phys. Chem. B* **2001**, *105*, 2785−2791.